Control of a Fuel Cell Based Z-Source Converter

Jin-Woo Jung, *Member, IEEE*, and Ali Keyhani, *Fellow, IEEE*

***Abstract*—This paper presents system modeling, modified space vector PWM implementation (MSVPWM), and control system design of a Z-source converter. For an electrical analysis of the fuel cell powered systems, the fuel cell system is modeled by an R–C circuit including its voltage–current polarization characteristics. A discrete-time state space equation is given to implement digital control and a space vector pulse-width modulation technique is modified to realize the shoot-through zero vectors that boost the dc-link voltage. Three discrete-time controllers and an asymptotic observer are designed.**

***Index Terms*—Digital control, distributed generation systems, dynamic model, fuel cells, space vector PWM, Z-source converter.**

I. Introduction

RECENT technological advances in small generators, power converter technology, and energy storage devices have provided a new opportunity for distributed generation systems (DGS). The DGS can offer improved service reliability, better economics and a reduced dependence on the local utility. Environmental friendly emerging technologies such as wind turbines, hydro turbines, photovoltaic cells, and fuel cells have also encouraged a more decentralized approach to power delivery due to environmental regulations regarding greenhouse gas emission [1]–[6]. Especially, the fuel cells can offer the prospect of supplying the world with safe, clean, efficient, sustainable electrical energy because they use hydrogen as a fuel and can continuously generate electric power as long as hydrogen and oxygen are available. Furthermore, the fuel cell development has been accelerated by investment of the automotive industry since it has an interest in clean energy for transportation.

A fuel cell is an electrochemical device that converts chemical energy directly into electric energy by reaction of hydrogen from the fuel and oxygen from the air. The fuel cells also produce water and heat by combining hydrogen with oxygen, and have 50% efficiency for only electricity but could reach 85% in the case of combined heat and power (CHP). Also, the fuel cells can be used for various applications such as stationary sites (buildings, hospitals, domestic utility, etc.), transportation (fuel cell vehicle), portable power (laptop, cell phone), and distributed power.

For practical realization of the fuel cell powered systems, slow dynamics of the fuel cells should be considered. Based on complicated physical and chemical processes, mathematical dynamic models of the fuel cells have been presented [7]–[13] for design of fuel cells. For a simplified dynamic analysis, a second-order model [14] or a first-order time delay circuit [15] has been proposed. For residential and automotive applications, the design and control of dc-to-dc boost converters and dc-to-ac inverters have been investigated to design low-cost and small-sized power converters [16]–[19]. However, the fuel cells are modeled by a dc voltage source and single-phase inverters are considered. In [20], [21], a Z-source converter that can boost a dc-link voltage by employing L–C impedance components and a shoot-through without any boost converter is proposed but it shows its operation under only a linear/heavy load and an open-loop control without considering the dynamics of the fuel cell system.

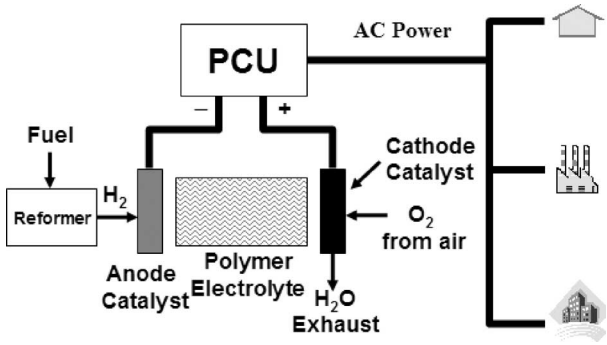

Fig. 1. Configuration of the fuel cell systems.

In addition, techniques to produce an ac output voltage with low THD in a three-phase PWM inverter have been proposed [22]–[25]. Real-time deadbeat controllers [22]–[24] have low THD for linear load and a fast transient response for load disturbances. However, it is known that these techniques have a high THD under nonlinear loads.

In this paper, system modeling, modified space vector PWM (MSVPWM) implementation, and control system design of a Z-source converter are presented. For considering dynamics of the fuel cell system, the fuel cell is modeled by an R–C circuit including its voltage–current polarization characteristics. A space vector PWM technique is modified to realize the shoot-through zero vectors that boost the dc-link voltage. Three discrete-time controllers and an asymptotic observer are designed to guarantee a fast, no-overshoot current response, a zero steady-state voltage and low THD under heavy/light loads, linear/nonlinear loads, and load changes. To verify the proposed control method, simulation studies using Matlab/Simulink are performed in a three-phase ac 208 V/60 Hz/10 kVA under various conditions.

II. Modeling of Fuel Cell

In the case of indirectly producing the hydrogen by the reformer, the fuel cell generation system consists of three parts: a reformer, stack, and power converters (Fig. 1). The reformer

Manuscript received September 24, 2005; revised September 24, 2005. This work was supported in part by the National Science Foundation under the grant NSF ECE 0501349. Paper no. TEC-00305-2004.

J. W. Jung is with the Samsung SDI Co., Yongin, Gyeonggi-Do 449-902, Korea (e-mail: jung.103@osu.edu).

A. Keyhani is with the Department of Electrical and Computer Engineering, The Ohio State University, Columbus, OH 43210 USA (e-mail: keyhani.1@osu.edu).

Digital Object Identifier 10.1109/TEC.2006.874232

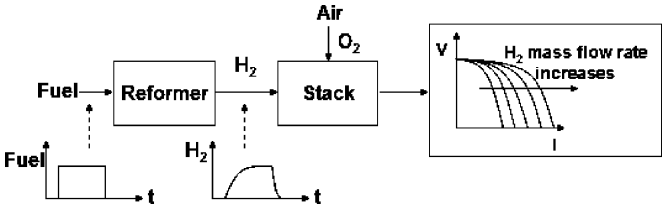

Fig. 2. Block diagram of reformer and stack.

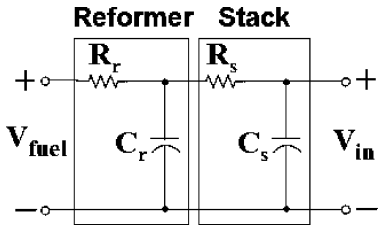

Fig. 3. Electrical equivalent circuit model of the fuel cell.

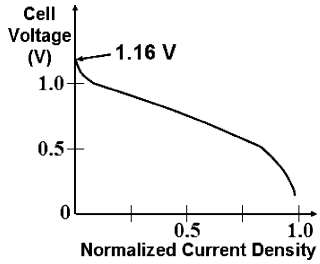

Fig. 4. Voltage–current characteristics of a cell.

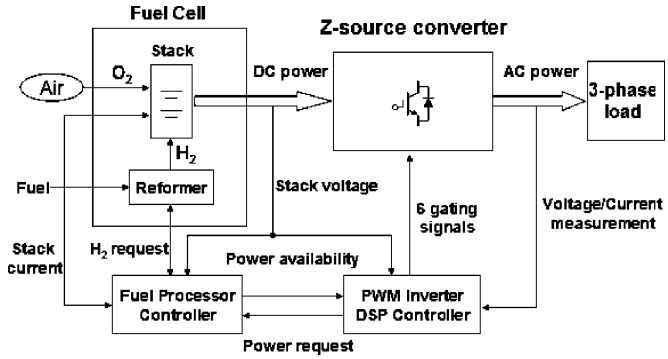

Fig. 5. System diagram of a fuel cell based Z-source converter.

produces hydrogen gas from fuels and then supplies it to the stack. The stack has many unit cells that are stacked in series or parallel to generate a higher voltage needed for their applications because one single cell that consists of electrolyte, separators, and plates, produces approximately 0.7 V dc. Also it generates dc electric power by an electrochemical reaction of hydrogen and oxygen. The power converters convert a low voltage dc from the fuel cell to a high voltage dc or a sinusoidal ac.

For dynamic modeling of the fuel cells, the reformer and stack that determine the dynamic response of the fuel cell systems are further described. Fig. 2 shows a block diagram of reformer and stack to illustrate the generation of dc power. The reformer affects dynamic response of the fuel cell system because it takes up several to tens of seconds to convert the fuel into the hydrogen depending on the demand of the load current. Thus, to investigate an overall operation of fuel cell powered systems, the dynamics of the reformer may be represented by a second-order model [14] or a first-order time delay model [15].

Dynamic response of the stack is considered to have faster response due to the electrochemical process of hydrogen and oxygen compared to that of the reformer. In Fig. 2, the output of the stack shows a family of voltage–current curves for various hydrogen mass flow rates. That is, the maximum cell current and stack voltage increase as the hydrogen mass flow rate increases. As a result, the dynamic response of the reformer and stack and a cell current voltage curve need to be modeled for more realistic analysis of the fuel cell systems.

In this paper, an R–C circuit model is used to realize slow dynamics caused by a chemical/electrical response of the reformer and stack as depicted in Fig. 3. In this figure, the reformer and stack are modeled by R_r and C_r, and R_s and C_s, respectively. The voltage–current polarization characteristics of the stack is also considered, and in this study, the V–I characteristics shown in Fig. 4 is used.

III. Configuration of Z-Source Converter for Fuel Cell Systems

The Z-source converter is based on a new concept different from a conventional dc-to-dc or dc-to-ac power converter [20]. In the conventional three-phase voltage source inverter (VSI), the shoot-through in which both power switches in a leg are at once turned on must be avoided because it causes a short circuit. The traditional three-phase VSI has eight switching vectors that consist of six active vectors (V_1–V_6) and two zero vectors (V_0, V_7). On the other hand, the Z-source converter has one more vector (i.e., the shoot-through zero vector) besides eight switching vectors. The Z-source converter utilizes the shoot-through to directly step up a dc source voltage without a boost dc/dc power converter. Thus, a boosted voltage rate depends on total duration (T_a) of the shoot-through zero vectors over one switching period (T_z).

Fig. 5 shows the total system diagram of a fuel cell based Z-source converter that consists of a reformer, stack, a fuel processor controller, a Z-source converter, a PWM inverter DSP controller, and a three-phase load.

As described in Fig. 5, the fuel processor controls the reformer to produce hydrogen for power requested from the PWM inverter DSP controller. The controller monitors the stack current and voltage to assure the proper operation of the fuel cell. The PWM inverter DSP controller communicates with the fuel cell processor to equalize power available from the stack to power requested by the load, controls the Z-source converter, and senses output voltages/currents for a closed-loop control.

Fig. 6 shows a detailed system configuration of a fuel cell powered Z-source converter. The filter capacitors (C_f) to filter

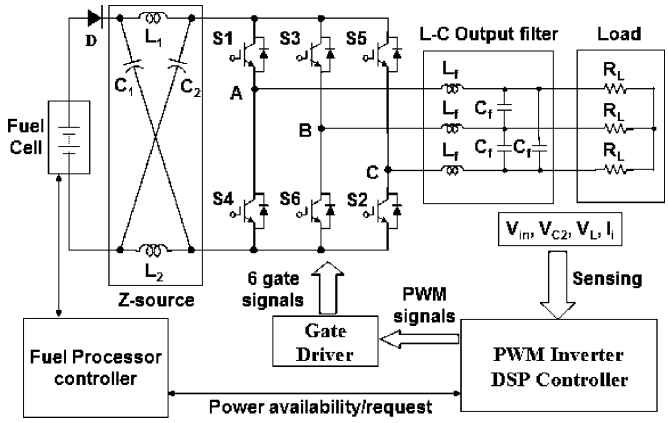

Fig. 6. Detailed configuration of the Z-source converter system.

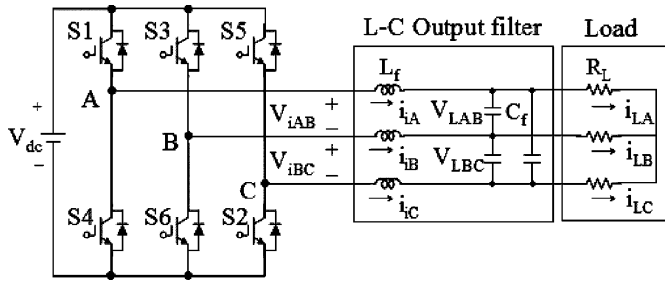

Fig. 7. Simplified circuit model of the Z-source converter.

out harmonics of the inverter output voltage due to the PWM technique are added to the conventional Z-source converter.

In Fig. 6, the system consists of a fuel cell, a diode, impedance components (L_1, L_2, C_1, and C_2), a three-phase inverter, an output filter (L_f and C_f), and a three-phase load (R_L). The diode between the fuel cell and Z-source converter is required to prevent a reverse current that can damage the fuel cell. Also, the output voltage ($V_{\rm in}$) of fuel cell, capacitor voltage (V_{C2}), inverter output current (I_i), and line-to-line load voltage (V_L) are measured to implement the feedback control.

IV. System Modeling/PWM Implementation

A. System Modeling

Fig. 7 shows a simplified circuit model of Fig. 6 for an analytic modeling of the Z-source converter using fuel cells.

Fig. 7 shows a system consisting of a dc voltage source, a three-phase inverter, an output filter (L_f and C_f), and a three-phase load. Notice that a fuel cell, a diode (D), and impedance components (L_1, L_2, C_1, and C_2) are replaced with a dc-link voltage source ($V_{\rm dc}$) for circuit modeling, and $V_{\rm dc}$ denotes the average dc-link voltage, which is also equal to the voltages (V_{C1} and V_{C2}) of two capacitors (C_1 and C_2).

The circuit model described in Fig. 7 uses the following quantities. The inverter output line-to-line voltage is represented by the vector $\mathbf{V}_i = [V_{iAB}\ V_{iBC}\ V_{iCA}]^T$, and the three-phase inverter output currents are i_{iA}, i_{iB}, and i_{iC}. Based on these currents, a vector is defined as $\mathbf{I}_i = [i_{iAB}\ i_{iBC}\ i_{iCA}]^T = [i_{iA} - i_{iB}\ \ i_{iB} - i_{iC}\ \ i_{iC} - i_{iA}]^T$. Also, the load line-to-line voltage and phase current vectors can be represented by $\mathbf{V}_L = [V_{LAB}\ V_{LBC}\ V_{LCA}]^T$ and $\mathbf{I}_L = [i_{LA}\ i_{LB}\ i_{LC}]^T$, respectively.

The L–C output filter yields the following state equations by KCL and KVL:

$$\frac{d\mathbf{V}_L}{dt} = \frac{1}{3C_f}\mathrm{I}_i - \frac{1}{3C_f}\mathbf{T}_i\mathbf{I}_L$$
$$\frac{d\mathbf{I}_i}{dt} = -\frac{1}{L_f}\mathbf{V}_L + \frac{1}{L_f}\mathbf{V}_i. \tag{1}$$

where

$$\mathbf{T}_i = \begin{bmatrix} 1 & -1 & 0 \\ 0 & 1 & -1 \\ -1 & 0 & 1 \end{bmatrix}.$$

To implement the space vector PWM, the above state equations can be transformed from the abc reference frame into stationary dq reference frame that consists of the horizontal (d) and vertical (q) axes. The relation between these two reference frames is below

$$\mathbf{f}_{dq0} = \mathbf{K}_s\mathbf{f}_{abc} \tag{2}$$

where

$$\mathbf{K}_s = \frac{2}{3}\begin{bmatrix} 1 & -1/2 & -1/2 \\ 0 & \sqrt{3}/2 & -\sqrt{3}/2 \\ 1/2 & 1/2 & 1/2 \end{bmatrix},$$

$\mathbf{f}_{dq0} = [f_d f_q f_0]^T$, $\mathbf{f}_{abc} = [f_a f_b f_c]^T$, and f denotes either a voltage or a current variable.

Using (2), the system model (1) in the abc reference frame can be transformed to (3) in the stationary dq reference frame as follows:

$$\frac{d\mathbf{V}_{Ldq}}{dt} = \frac{1}{3C_f}\mathbf{I}_{idq} - \frac{1}{3C_f}\mathbf{T}_{idq}\mathbf{I}_{Ldq}$$
$$\frac{d\mathbf{I}_{idq}}{dt} = -\frac{1}{L_f}\mathbf{V}_{Ldq} + \frac{1}{L_f}\mathbf{V}_{idq} \tag{3}$$

where

$$\mathbf{T}_{idq} = [\mathbf{K}_s\mathbf{T}_i\mathbf{K}_s^{-1}]_{\rm row,column,1,2} = \frac{3}{2}\begin{bmatrix} 1 & \frac{-1}{\sqrt{3}} \\ \frac{1}{\sqrt{3}} & 1 \end{bmatrix}.$$

The given plant model (3) can be expressed as the following continuous-time state space equation

$$\dot{\mathbf{X}}(t) = \mathbf{A}\mathbf{X}(t) + \mathbf{B}\mathbf{u}(t) + \mathbf{E}\mathbf{d}(t) \tag{4}$$

where

$$\mathbf{X} = \begin{bmatrix} \mathbf{V}_{Ldq} \\ \mathbf{I}_{idq} \end{bmatrix}_{4\times1}, \quad \mathbf{A} = \begin{bmatrix} 0_{2\times2} & \frac{1}{3C_f}I_{2\times2} \\ -\frac{1}{L_f}I_{2\times2} & 0_{2\times2} \end{bmatrix}_{4\times4},$$
$$\mathbf{B} = \begin{bmatrix} 0_{2\times2} \\ \frac{1}{L_f}I_{2\times2} \end{bmatrix}_{4\times2}, \quad \mathbf{u} = [\mathbf{V}_{idq}]_{2\times1},$$
$$\mathbf{E} = \begin{bmatrix} -\frac{1}{3C_f}\mathbf{T}_{idq} \\ 0_{2\times2} \end{bmatrix}_{4\times2}, \quad \mathbf{d} = [\mathbf{I}_{Ldq}]_{2\times1}.$$

Note that the line-to-line load voltage $\mathbf{V}_{Ldq}$ and inverter output current $\mathbf{I}_{idq}$ are the state variables of the system, the inverter

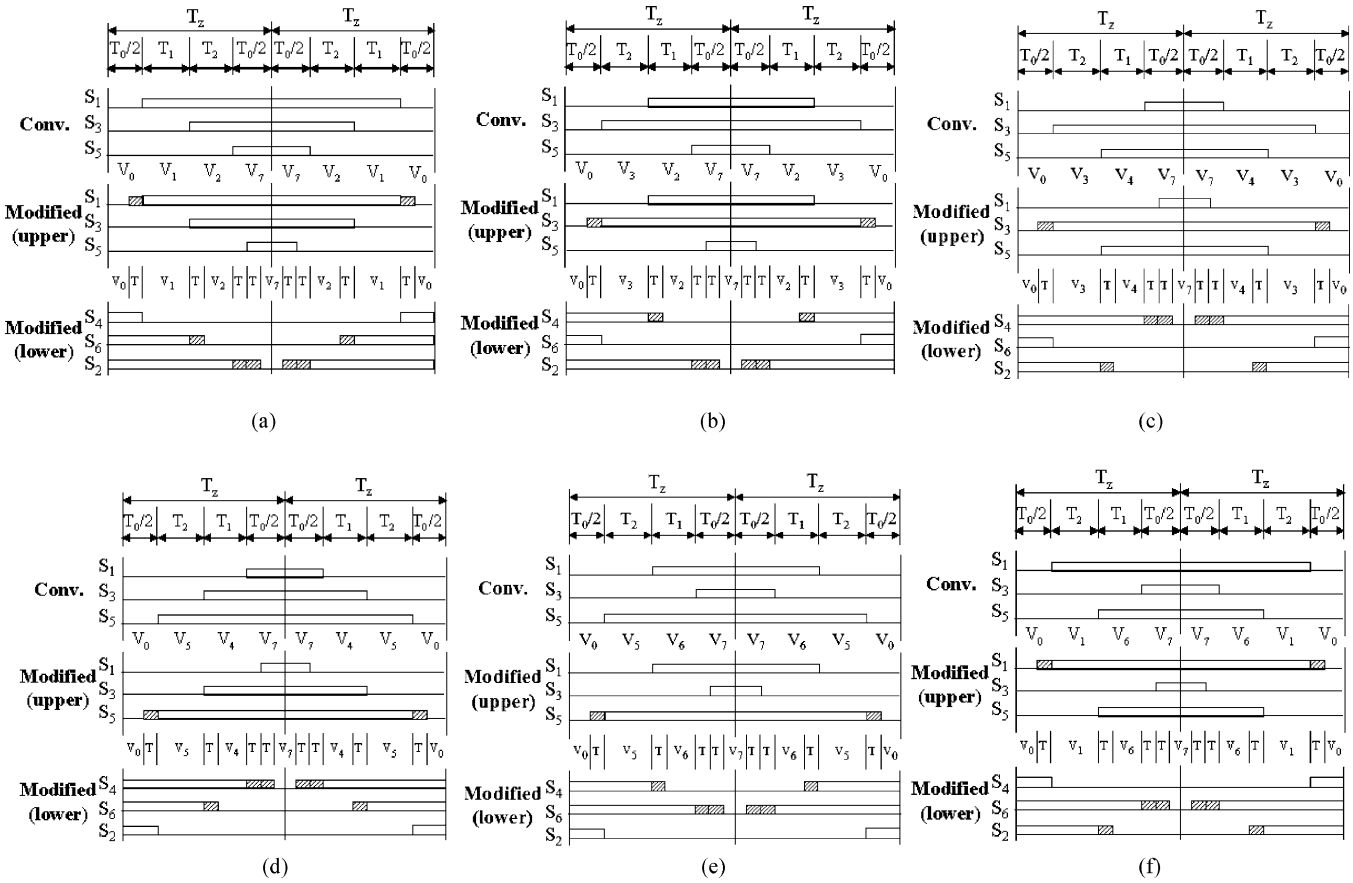

Fig. 8. Modified SVPWM implementation. (a) Sector 1. (b) Sector 2. (c) Sector 3. (d) Sector 4. (e) Sector 5. (f) Sector 6.

output line-to-line voltage $\mathbf{V}_{idq}$ is the control input $(\mathbf{u})$, and the load current $\mathbf{I}_{Ldq}$ is defined as the disturbance $(\mathbf{d})$.

B. Space Vector PWM Implementation

For realization of the Z-source converter to utilize the shoot-through, the conventional SVPWM technique should be modified. Fig. 8 shows both the conventional and modified switching patterns for the Z-source converter at each sector. In this figure, a new duration (T) should be added to the switching time $(T_1, T_2,$ and $T_0)$ of the traditional SVPWM in order to boost the dc-link voltage of the Z-source converter and to generate the sinusoid ac output voltage. For implementation of the modified space vector PWM, the switching time of the upper switches and lower switches in a three-phase inverter is summarized in Table I below.

In the Z-source converter, the peak value of phase-a inverter output voltage can be written as [20]

$$V_{a\_p} = M\frac{V_{p\_dc}}{2} = MK\frac{V_{in}}{2} \tag{5}$$

where

$$K = \frac{T_z}{T_b - T_a} = \frac{1}{1 - 2\frac{T_a}{T_z}} \geq 1$$

K is called a boost factor and M and V_{p_dc} denote the modulation index and the peak dc-link voltage, respectively,

TABLE I
SWITCHING TIME DURATION AT EACH SECTOR

Sector	Upper (S1, S3, S5)	Lower (S4, S6, S2)
1	S1 = T1 + T2 + T0/2 + T S3 = T2 + T0/2 S5 = T0/2 – T	S4 = T0/2 S6 = T1 + T0/2 + T S2 = T1 + T2 + T0/2 + 2T
2	S1 = T1 + T0/2 S3 = T1 + T2 + T0/2 + T S5 = T0/2 – T	S4 = T2 + T0/2 + T S6 = T0/2 S2 = T1 + T2 + T0/2 + 2T
3	S1 = T0/2 – T S3 = T1 + T2 + T0/2 + T S5 = T2 + T0/2	S4 = T1 + T2 + T0/2 + 2T S6 = T0/2 S2 = T1 + T0/2 + T
4	S1 = T0/2 – T S3 = T1 + T0/2 S5 = T1 + T2 + T0/2 + T	S4 = T1 + T2 + T0/2 + 2T S6 = T2 + T0/2 + T S2 = T0/2
5	S1 = T2 + T0/2 S3 = T0/2 – T S5 = T1 + T2 + T0/2 + T	S4 = T1 + T0/2 + T S6 = T1 + T2 + T0/2 + 2T S2 = T0/2
6	S1 = T1 + T2 + T0/2 + T S3 = T0/2 – T S5 = T1 + T0/2	S4 = T0/2 S6 = T1 + T2 + T0/2 + 2T S2 = T2 + T0/2 + T

$T_z = T_a + T_b; T_z$ is the switching period, T_a is the total duration of shoot-through zero vectors during T_z, and T_b is the total duration of nonshoot-through switching vectors during T_z.

From (5), the peak value of inverter output voltage (V_{a_p}) definitely depends on both the modulation index (M) and the boost factor (K), and the boost factor (K) is determined by

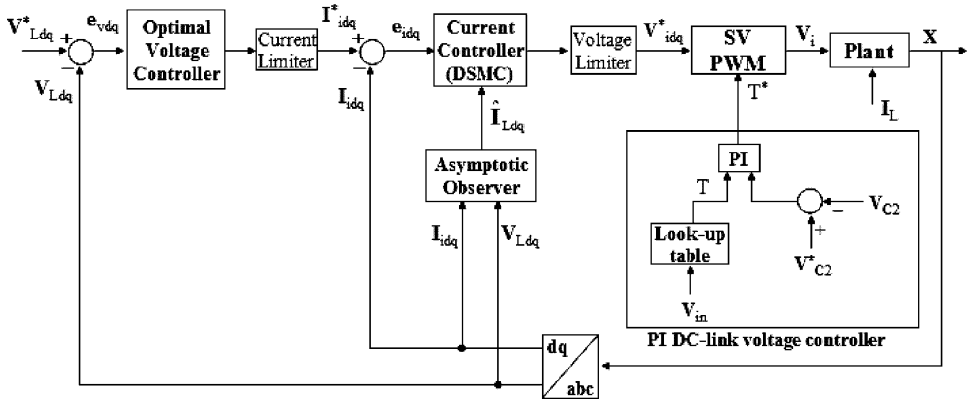

Fig. 9. Total control system block diagram.

a ratio T_a/T_z. Moreover, sum of the modulation index ($M = T_b/T_z$) and the ratio T_a/T_z is always equal to unity.

Thus, the boosted rate of the dc-link voltage is dependent on the total duration ($T_a = 3T$) of shoot-through zero vectors that simultaneously turn on both power switches in a leg. In Fig. 8, each phase still switches on and off once per switching cycle (T_z), and has only one shoot-through zero state (T) over one period (T_z) in any sector without the change of total zero vectors (V_0, V_7, and T) and total nonzero switching vectors (V_1–V_6). Even if the output voltage of inverter and dc-link voltage can be controlled by adjusting T_a, the maximum available shoot-through interval (T_a) to boost the dc-link voltage (v_i) is limited by the zero vector duration ($T_0/2$) which is determined by the modulation index ($M = a(4/3)$).

V. Control System Design

Fig. 9 shows a block diagram of the control system proposed for the fuel cell based Z-source converter. As shown in this figure, the overall system has three feedback controllers and an asymptotic observer. In the following sections, design of each controller will be described in detail.

A. Discrete-Time Sliding Mode Current Controller

A discrete-time sliding mode control (DSMC) with the asymptotic observer is used for current regulation in an inner loop because of the fast and no-overshoot response [28].

Using the asymptotic observer which estimates the load current ($\mathbf{I}_{Ldq}$) defined as the disturbance, the load current can be estimated as follows:

$$\begin{cases} \hat{\mathbf{X}}_a(k+1) = \mathbf{A}_a^*\hat{\mathbf{X}}_a(k) + \mathbf{A}_b^*\mathbf{X}_b(k) - \mathbf{A}_a^{**}\mathbf{X}_a(k) \\ \hat{\mathbf{d}}(k) = \hat{\mathbf{I}}_{Ldq}(k) = L_1(\hat{\mathbf{X}}_a(k) - \mathbf{X}_a(k)) \end{cases} \tag{6}$$

where

$$\hat{\mathbf{X}}_a = [\hat{\mathbf{V}}_{Ldq}], \quad \mathbf{X}_b = [\mathbf{I}_{idq}], \quad \mathbf{X}_a = [\mathbf{V}_{Ldq}],$$

$$\mathbf{A}_a^* = e^{\mathbf{A}_a T_z}, \quad \mathbf{A}_b^* = \int_0^{T_z} e^{\mathbf{A}_a(T_z-r)}\mathbf{A}_b d\tau,$$

$$\mathbf{A}^{**} = \int_0^{T_z} e^{\mathbf{A}_a(T_z-r)}\mathbf{A}_a d\tau, \mathbf{A}_a = \left[-\frac{L_1}{3C_f}\mathbf{T}_{idq}\right],$$

$$\mathbf{A}_b = \left[\frac{1}{3C_f} I_{2\times 2}\right], \quad L_1 = \text{observer gain}.$$

With the information of the disturbance obtained from the observer, the discrete-time state space equation of the system (4) for design of a current controller can be expressed as

$$\begin{cases} \mathbf{X}(k+1) = \mathbf{A}^*\mathbf{X}(k) + \mathbf{B}^*\mathbf{u}(k) + \mathbf{E}^*\hat{\mathbf{d}}(k) \\ \mathbf{y}_1(k) = \mathbf{C}_1\mathbf{X}(k) \\ \mathbf{e}_{idq}(k) = \mathbf{y}_1(k) - \mathbf{y}_{1\_\mathrm{ref}}(k) \end{cases} \tag{7}$$

where

$$\mathbf{y}_1 = [\mathbf{I}_{idq}], \quad \mathbf{y}_{1\_\mathrm{ref}} = [\mathbf{I}_{idq}^*], \quad \mathbf{C}_1 = \begin{bmatrix} 0 & 0 & 1 & 0 \\ 0 & 0 & 0 & 1 \end{bmatrix},$$

$$\hat{\mathbf{d}} = [\hat{\mathbf{I}}_{Ldq}], \quad \mathbf{A}^* = e^{\mathbf{A}T_z}, \quad \mathbf{B}^* = \int_0^{T_z} e^{\mathbf{A}(T_z-\tau)}\mathbf{B}\, d\tau,$$

$$\mathbf{E}^* = \int_0^{T_z} e^{\mathbf{A}(T_z-\tau)}\mathbf{E} d\tau.$$

In order to control the output $\mathbf{y}_1(k)$ to follow the reference $\mathbf{y}_{1\_\mathrm{ref}}(k)$, a sliding mode manifold can be selected below

$$\mathbf{s}(k) = \mathbf{y}_1(k) - \mathbf{y}_{1\_\mathrm{ref}}(k) = \mathbf{C}_1\mathbf{X}(k) - \mathbf{y}_{1\_\mathrm{ref}}(k). \tag{8}$$

Therefore, discrete-time sliding mode can be reached if the control input $u(k)$ is designed as the solution of

$$\begin{aligned} \mathbf{s}(k+1) &= \mathbf{y}_1(k+1) - \mathbf{y}_{1\_\mathrm{ref}}(k+1) \\ &= \mathbf{C}_1\mathbf{A}^*\mathbf{X}(k) + \mathbf{C}_1\mathbf{B}^*\mathbf{u}(k) + \mathbf{C}_1\mathbf{E}^*\hat{\mathbf{d}}(k) \\ &\quad - \mathbf{y}_{1\_\mathrm{ref}}(k+1) = 0. \end{aligned} \tag{9}$$

The control law that satisfies (9) and yields motion in the manifold $s(k) = 0$ is called "equivalent control" and is given by

$$\mathbf{u}_{\mathrm{eq}}(k) = (\mathbf{C}_1\mathbf{B}^*)^{-1}(\mathbf{I}_{idq}^*(k) - \mathbf{C}_1\mathbf{A}^*\mathbf{X}(k) - \mathbf{C}_1\mathbf{E}^*\hat{\mathbf{d}}(k)). \tag{10}$$

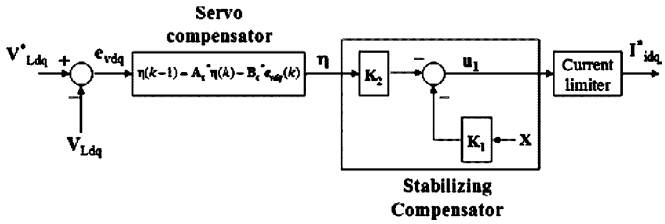

Fig. 10. Discrete-time voltage controller.

If the control input is limited by $\|\mathbf{u}(k)\| \le u_0$, then the following modified control input can be applied:

$$\mathbf{u}(k) = \begin{cases} \mathbf{u}_{\rm eq}(k) & \text{for } \|\mathbf{u}_{\rm eq}(k)\| \le u_0 \\ \frac{u_0}{\|\mathbf{u}_{\rm eq}(k)\|}\mathbf{u}_{\rm eq}(k) & \text{for } \|\mathbf{u}_{\rm eq}(k)\| > u_0 \end{cases}. \tag{11}$$

With control law (11), the discrete-time sliding mode can be reached after a finite number of steps and the control voltage limit $\mathbf{u}_0$ is also determined by the SVPWM inverter.

B. Discrete-Time Optimal Voltage Controller

As shown in Fig. 10, a discrete-time voltage controller that consists of a servo-compensator with the internal model principle and a stabilizing compensator with the optimal control is used for voltage regulation in an outer loop due to its capability to perform zero steady-state tracking error under unknown load and to eliminate harmonics of any specified frequencies with guaranteed system stability [26], [27]. Also, the current command signal $(\mathbf{I}_{\rm cmd,idq})$ is limited by maximum current to protect the system under over-current.

Since the dynamics of the DSMC is included in the inner loop, its model has to be combined with the original plant. After the dynamics (10) of the DSMC is included in (7), the overall plant can be expressed as

$$\begin{cases} \mathbf{X}(k+1) = \mathbf{A}_d\mathbf{X}(k) + \mathbf{B}_d\mathbf{u}_1(k) + \mathbf{E}_d\hat{\mathbf{d}}(k), \\ \mathbf{y}_d(k) = \mathbf{C}_d\mathbf{X}(k) \end{cases} \tag{12}$$

where

$$\mathbf{y}_d = [\mathbf{V}_{Ldq}], \quad \mathbf{C}_d = [I_{2\times2} \quad 0_{2\times2}],$$
$$\mathbf{A}_d = \mathbf{A}^* - \mathbf{B}^*(\mathbf{C}_1\mathbf{B}^*)^{-1}\mathbf{C}_1\mathbf{A}^*, \quad \mathbf{B}_d = \mathbf{B}^*(\mathbf{C}_1\mathbf{B}^*)^{-1},$$
$$\mathbf{E}_d = \mathbf{E}^* - \mathbf{B}^*(\mathbf{C}_1\mathbf{B}^*)^{-1}\mathbf{C}_1\mathbf{E}^*, \quad \mathbf{u}_1(k) = \mathbf{I}_{\rm cmd,idq}(k).$$

For the above system (12), we assume the tracking/disturbance poles are $\pm j\omega_1, \pm j\omega_2, \pm j\omega_3, \ldots$ (i.e., representing sinusoidal signals with fundamental frequency ω_1 and harmonic frequencies $\omega_2,\ \omega_3, \ldots$). If the tracking/disturbance poles to be considered are $\pm j\omega_1, \pm j\omega_2$, and $\pm j\omega_3$, the continuous-time servo-compensator is

$$\dot{\boldsymbol{\eta}} = \mathbf{A}_c\boldsymbol{\eta} + \mathbf{B}_c\mathbf{e}_{vdq}, \tag{13}$$

where

$$\mathbf{e}_{vdq} = \mathbf{V}^*_{Ldq} - \mathbf{V}_{Ldq}, \mathbf{A}_c = \begin{bmatrix} \mathbf{A}_{c1} & 0_{4\times4} & 0_{4\times4} \\ 0_{4\times4} & \mathbf{A}_{c2} & 0_{4\times4} \\ 0_{4\times4} & 0_{2\times2} & \mathbf{A}_{c3} \end{bmatrix}_{12\times12},$$
$$B_c = \begin{bmatrix} \mathbf{B}_{c1} \\ \mathbf{B}_{c2} \\ \mathbf{B}_{c3} \end{bmatrix}_{12\times2}, \mathbf{A}_{ci} = \begin{bmatrix} 0_{2\times2} & I_{2\times2} \\ -\omega_i^2\cdot I_{2\times2} & 0_{2\times2} \end{bmatrix}_{4\times4},$$
$$\mathbf{B}_{ci} = \begin{bmatrix} 0_{2\times2} \\ I_{2\times2} \end{bmatrix}_{4\times2},$$

and $\omega_i (i = 1, 2, 3), \omega_1 = \omega, \omega_2 = 5\omega, \omega_3 = 7\omega$.

Note that only the dominant 5th and 7th harmonics are chosen as the disturbance poles because the voltage harmonics such as an odd multiple of 3 and even harmonics are suppressed in a three-phase inverter.

The discrete form of (13) is

$$\boldsymbol{\eta}(k+1) = \mathbf{A}^*_c\boldsymbol{\eta}(k) + \mathbf{B}^*_c\mathbf{e}_{vdq}(k) \tag{14}$$

where

$$\mathbf{A}^*_c = e^{\mathbf{A}_cT_z}, \quad \mathbf{B}^*_c = \int_0^{T_z} e^{\mathbf{A}_c(T_z-\tau)}\mathbf{B}_c d\tau.$$

Therefore, an augmented system combining both the plant (12) and the servo-compensator (14) is

$$\hat{\mathbf{X}}(k+1) = \hat{\mathbf{A}}\hat{\mathbf{X}}(k) + \hat{\mathbf{B}}\mathbf{u}_1(k) + \hat{\mathbf{E}}_1\hat{\mathbf{d}}(k) + \hat{\mathbf{E}}_2\mathbf{y}_{d\_\rm ref}(k) \tag{15}$$

where

$$\hat{\mathbf{X}}(k) = \begin{bmatrix} \mathbf{X}(k) \\ \boldsymbol{\eta}(k) \end{bmatrix}, \quad \hat{\mathbf{A}} = \begin{bmatrix} \mathbf{A}_d & 0 \\ -\mathbf{B}^*_c\mathbf{C}_d & \mathbf{A}^*_c \end{bmatrix},$$
$$\hat{\mathbf{B}} = \begin{bmatrix} \mathbf{B}_d \\ 0 \end{bmatrix}, \quad \hat{\mathbf{E}}_1 = \begin{bmatrix} \mathbf{E}_d \\ 0 \end{bmatrix}, \quad \hat{\mathbf{E}}_2 = \begin{bmatrix} 0 \\ \mathbf{B}^*_c \end{bmatrix},$$
$$\mathbf{u}_1(k) = \mathbf{I}_{\rm cmd,idq}(k), \quad \hat{\mathbf{d}}(k) = \hat{\mathbf{I}}_{Ldq}(k),$$
$$\mathbf{y}_{\rm d\_ref}(k) = \mathbf{V}^*_{Ldq}(k).$$

The stabilizing compensator which yields the control signal $\mathbf{u}_1$ ensures the stability and desirable performance of the overall system through a feedback gain $\mathbf{K}$ which minimizes a discrete linear quadratic performance index

$$j_\varepsilon = \sum_{k=0}^{\infty} \hat{\mathbf{X}}^T(k)\mathbf{Q}\hat{\mathbf{X}}(k) + \varepsilon\mathbf{u}_1^T(k)\mathbf{u}_1(k) \tag{16}$$

where $\mathbf{Q}$ is a symmetrical positive-definite matrix and $\varepsilon > 0$ is a small number.

The optimal gain matrix $\mathbf{K}$ is obtained by solving the algebraic Riccati equation for (15). As a result, the control input (u_1) can be given as

$$\mathbf{u}_1(k) = -\mathbf{K}\hat{\mathbf{X}}(k) = -[\mathbf{K}_1 \quad \mathbf{K}_2]\begin{bmatrix} \mathbf{X}(k) \\ \boldsymbol{\eta}(k) \end{bmatrix}$$
$$= -\mathbf{K}_1\mathbf{X}(k) - \mathbf{K}_2\boldsymbol{\eta}(k). \tag{17}$$

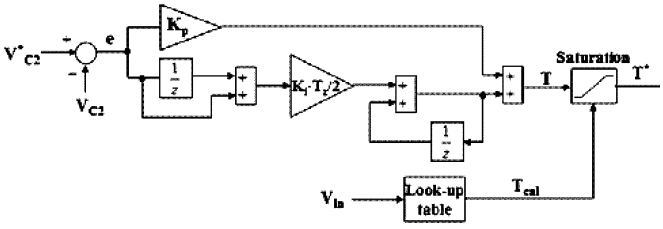

Fig. 11. Discrete PI controller to regulate the DC-link average voltage.

C. Discrete PI dc-Link Voltage Controller

Finally, a discrete PI voltage controller based on Tustin's method for approximation to integration is used to regulate the average voltage of dc-link in Fig. 11.

The equation for the PI controller is given (18) where K_p is the proportional gain, and K_i is the integral gain.

As shown in Fig. 11, one of the capacitor voltages (V_{C1}, V_{C2}) is measured for the feedback control, and an error between the desired voltage $(\mathbf{V}^*_{c2})$ and sensed voltage (V_{C2}) is used as an input of the controller. Moreover, the output voltage $(V_{\rm in})$ of the fuel cell is sensed, and then duration $(T_{\rm cal} = T_a/3)$ of shoot-through zero vectors is calculated by look-up table according to the magnitude of the fuel cell output voltage. Equation (19) shows how $T_{\rm cal}$ is theoretically calculated assuming that a desired capacitor voltage (V_{C2}) is 340 V and a switching period $(T_z = 185.2\ \mu s)$. That is, the parameters K, M, a, and T can be calculated as follow:

1). When $V_{\rm in} = 130$ V and $P = 10$ kW: $T_a/T_z = 0.3814$, $K = 4.2158, M = 0.6186, a = 0.4639, T = 23.54\mu$s;
2). When $V_{\rm in} = 300$ V and $P = 0.5$ kW: $T_a/T_z = 0.1053$, $K = 1.2668, M = 0.8947, a = 0.671, T = 6.5\mu$s.

$$V_{c1} = V_{c2} = \frac{T_b}{T_b - T_a} = \frac{T_z - T_a}{T_z - 2T_a} = \frac{1 - T_a/T_z}{1 - 2T_a/T_z} V_{\rm in}. \tag{19}$$

Therefore

$$T_a/T_z = \frac{V_{c1} - V_{\rm in}}{2V_{c1} - V_{\rm in}} \Rightarrow K = \frac{1}{1 - 2T_a/T_z}$$
$$M(= T_b/T_z) = 1 - T_a/T_z \Rightarrow a = 3M/4$$
$$T = T_a/3$$

Fig. 12 shows relationship between $V_{\rm in}, T_a/T_z$, and K, and as we expect, T_a/T_z and K decrease as the output voltage $(V_{\rm in})$ of the fuel cell increases.

The calculated shoot-through duration $(T_{\rm cal})$ is utilized in a saturation block in order to limit the final output (T) of the discrete PI controller. This controller should regulate the average dc-link output voltage to the desired value and the shoot-through duration (T) should be confined to a reasonable value that can guarantee accurately the required boosted dc-link voltage. As illustrated in Table I, the reference duration $(T^* = T^*_a/3)$ of shoot-through zero states is directly added to or subtracted from the conventional switching patterns of SVPWM to boost the average dc-link voltage.

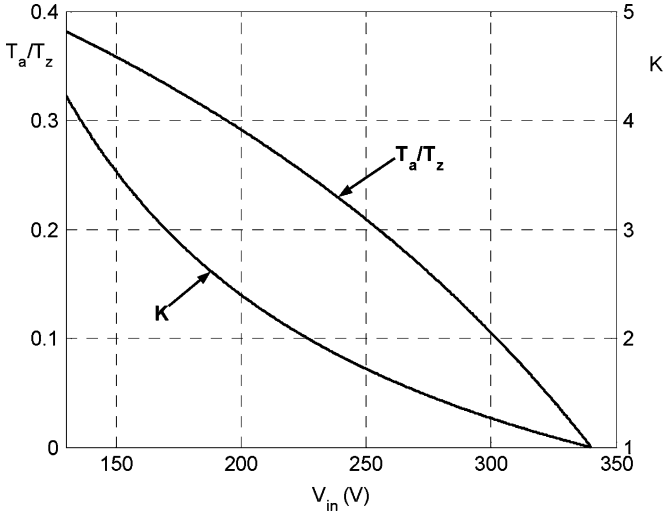

Fig. 12. Relationship between $V_{\rm in}, T_a/T_z$, and K.

TABLE II
SYSTEM PARAMETERS FOR SIMULATIONS

Fuel Cell Output Voltage	V_{in} = 130 ~ 300 V
Desired Average DC-link Voltage	V_{C2} = 340 V
Output Rated Power	P_{out} = 10 kVA
Impedance Components	$L_1 = L_2$ = 200 μH, $C_1 = C_2$ = 1000 μF
Inverter Output Filters	L_f = 1000 μH, C_f = 200 μF
AC Output Voltage	$V_{L,\,RMS}$ = 208 V (L-L), f = 60 Hz
Switching/Sampling Period	T_z = 1/(5.4 kHz)

VI. SIMULATION RESULTS

To validate the effectiveness of the proposed model and control strategy, a simulation test bed using Matlab/Simulink is constructed for an ac 208 V (L–L)/60 Hz/10 kVA, and simulation studies are performed under both linear and nonlinear loads. The system parameters are given in Table II.

In this paper, the simulations are implemented under various conditions: a heavy/light load, a linear/nonlinear load, and a load change. In case of the heavy load (10 kW), we assume that the output voltage of fuel cell is 130 V, while in case of the light

$$\begin{cases} e(k) = \mathbf{V}^*_{c2}(k) - \mathbf{V}_{c2}(k) \\ T(k) = T(k-1) + K_p(e(k) - e(k-1)) + K_i \frac{T_z}{2}(e(k) + e(k-1)) \end{cases} \tag{18}$$

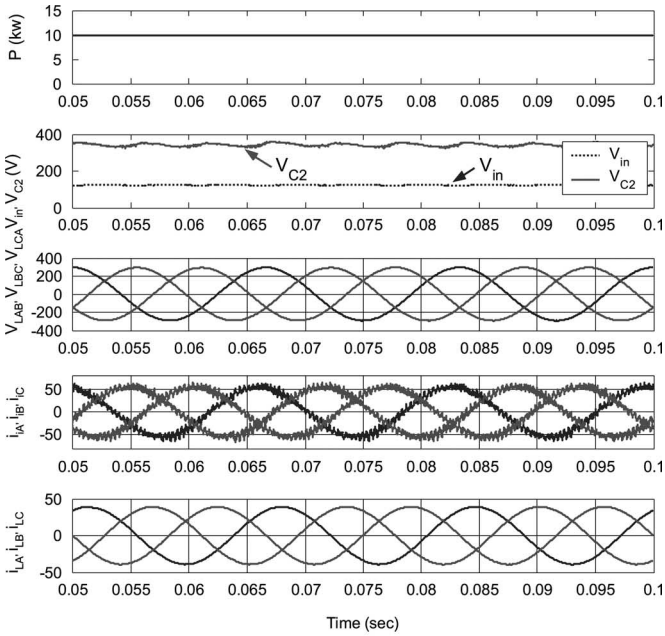

(a)

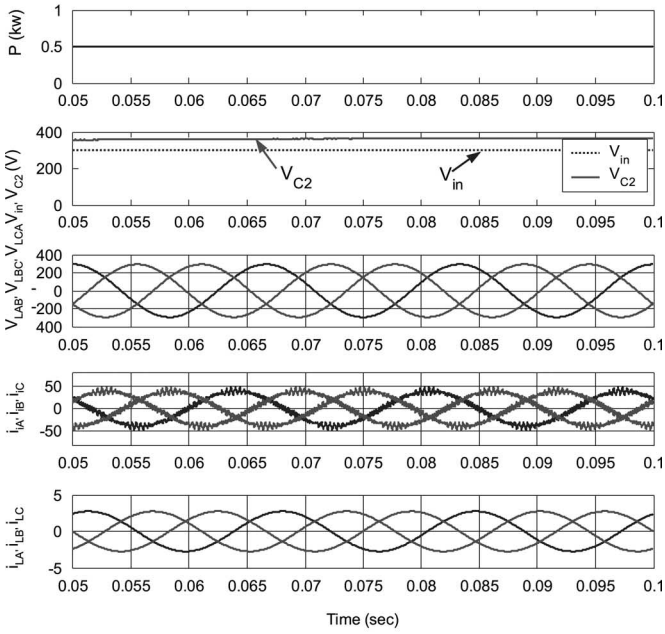

(b)

Fig. 13. Simulation results under a linear load. (a) 130 V and 10 kW. (b) 300 V and 0.5 kW.

load (0.5 kW) that of fuel cell is 300 V. The linear load consists of a resistor, whereas the nonlinear load is composed of a three-phase inductor (2 mH), a three-phase diode bridge, a dc-link capacitor $(800\ \mu F)$, and a resistor $(7\ \Omega)$. From Fig. 4, when the load increases from 5 to 10 kW, we assume that the output voltage of the fuel cell is changed from 250 to 130 V. On the other hand, when the load decreases from 10 to 5 kW, the output voltage of the fuel cell is changed from 130 to 250 V. In addition, we assume that the parameters of the reformer and stack are:

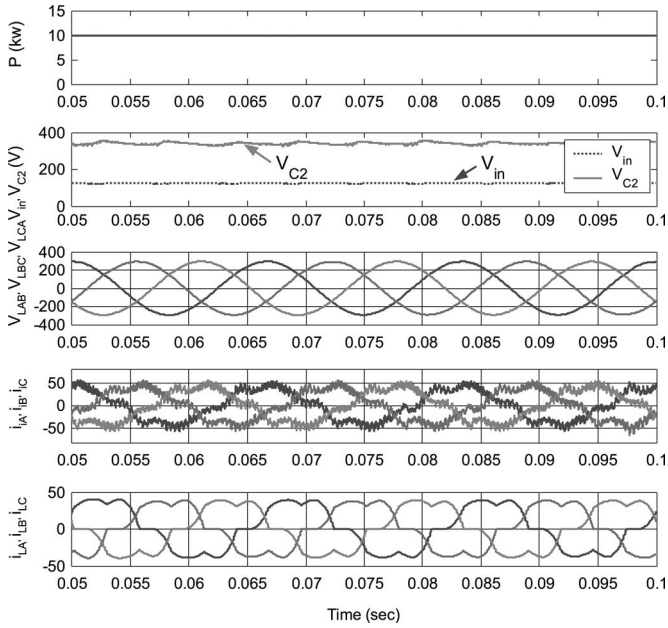

Fig. 14. Simulation results under a nonlinear load.

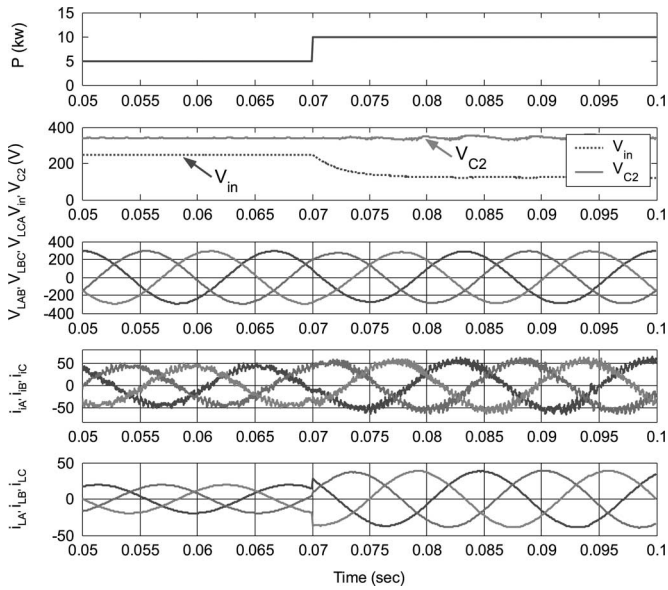

Fig. 15. Simulation results when the load increases.

$R_r = 0.05\,\Omega$ and $C_r = 42.8$ mF, $R_s = 0.02\,\Omega$ and $C_s = 4.2$ mF to show a general dynamic response of the fuel cell [15].

Fig. 13 shows simulation waveforms under the heavy and light load: (a) heavy load (130 V and 10 kW), and (b) light load (300 V and 0.5 kW).

Fig. 14 shows simulation results under the nonlinear load (130 V and 7 Ω). Figs. 15 and 16 show the results under a load change: load increase and decrease, respectively. Also, Fig. 17 shows PWM waveforms of six-power transistors at heavy load to regulate the average dc-link voltage (V_{C2}) as well as the inverter output voltage, and the shoot-through in which both power switches in a leg are simultaneously turned on is definitely

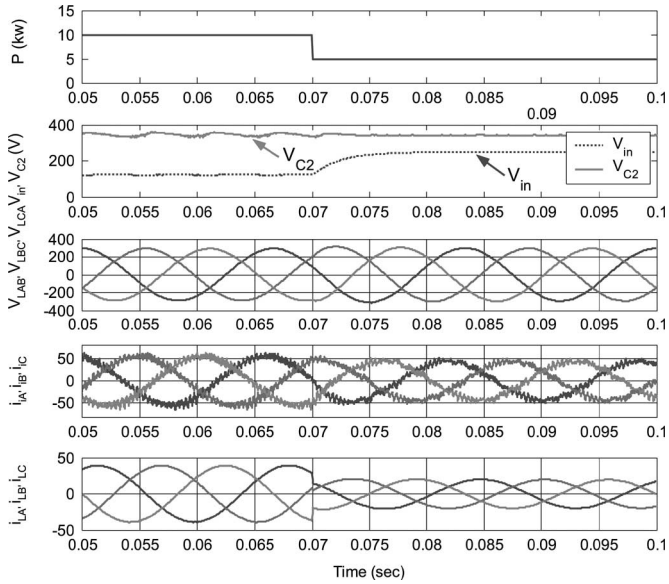

Fig. 16. Simulation results when the load decreases.

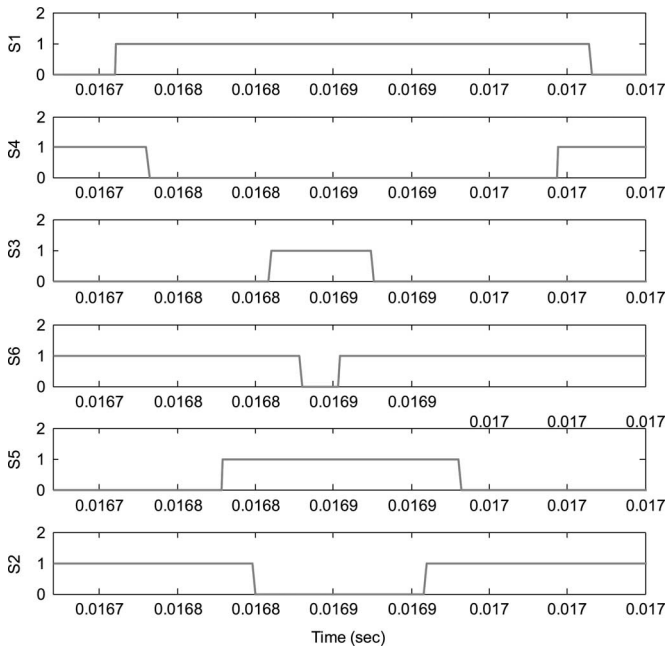

Fig. 17. PWM waveforms at heavy load.

shown. Fig. 18 shows the real load current (i_{LA}) and estimated load current (i^*_{LA})under the heavy load (130 V/10 kVA): upper (linear load) and lower (nonlinear load).

In Figs. 13 to 16, each figure indicates (a) Power request at 70 ms, (b) Output voltage of the fuel cell $(V_{\rm in})$ and capacitor (V_{C2}), (c) Load line to line voltages $(V_{LAB}, V_{LBC}, V_{LCA})$, (d) Inverter output phase currents (i_{iA}, i_{iB}, i_{iC}), and (e) Load phase currents (i_{LA}, i_{LB}, i_{LC}). As shown in Figs. 15 and 16 (b), (d), a good voltage regulation of capacitor voltage (V_{C2}) is presented in spite of a slow change of the fuel cell output voltage and load changes.

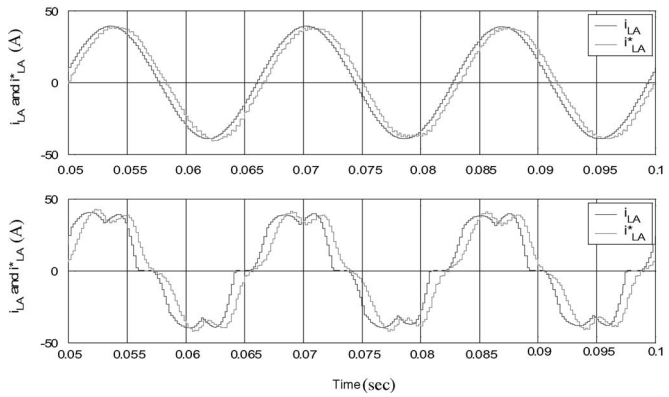

Fig. 18. Estimated load current under a heavy load.

VII. Conclusion

The paper studies system modeling, modified space vector PWM implementation and design of a closed-loop controller of the Z-source converter employing L–C passive components. An R–C circuit model is used to realize slow dynamics caused by a chemical/electrical response of the reformer and stack of the fuel cells, and a voltage–current polarization curve of a cell is also considered. A space vector pulse-width modulation technique is modified to realize the shoot-through zero vectors that boost the dc-link voltage.Furthermore, a new control algorithm is presented which can guarantee a fast, no-overshoot current response, a zero steady-state voltage, and low Total Harmonic Distortion (THD).

First of all, the Z-source converter does not need power devices, voltage/current sensors and a DSP controller as part of a dc/dc boost converter. As a result, when comparing the Z-source converter with dc/dc boost converter plus voltage source inverter (VSI), it has some advantages such as increased efficiency, enhanced reliability, and lower cost at the expense of the added complexity in control. Especially, the efficiency can be improved in the range of several percent over the conventional dc/dc boost converter plus VSI because of no switching and conduction losses due to power switches of the dc/dc boost converter. Also, the total system cost can be reduced by tens of percent because the power devices, sensors and DSP controller to boost dc-link voltage are removed.

To validate the proposed method, a system with a three-phase ac 208 V/60 Hz/10 kVA is simulated using Matlab/Simulink under various operating conditions such as heavy/light loads, linear/nonlinear loads, and load changes.

References

[1] M. N. Marwali and A. Keyhani, "Control of distributed generation systems, Part I: Voltages and currents control," *IEEE Trans. Power Electron.*, vol. 19, pp. 1541–1550, Nov. 2004.

[2] M. N. Marwali, J. W. Jung, and A. Keyhani, "Control of distributed generation systems, Part II: Load sharing control," *IEEE Trans. Power Electron.*, vol. 19, pp. 1551–1561, Nov. 2004.

[3] A. A. Chowdhury, S. K. Agarwal, and D. O. Koval, "Reliability modeling of distributed generation in conventional distribution systems planning and analysis," *IEEE Trans. Ind. Appl.*, vol. 39, pp. 1493–1498, Sep.–Oct. 2003.

[4] J. L. Del Monaco, "The role of distributed generation in the critical electric power infrastructure," *IEEE Power Eng. Soc. Winter Meet.*, vol. 1, pp. 144–145, Jan.–Feb. 2001.
[5] L. Philipson, "Distributed and dispersed generation: Addressing the spectrum of consumer needs," *IEEE Power Eng. Soc. Summer Meet.*, vol. 3, pp. 1663–1665, Jul. 2000.
[6] J. Gutierrez-Vera, "Use of renewable sources of energy in Mexico," *IEEE Trans. Energy Convers.*, vol. 9, pp. 442–450, Sep. 1994.
[7] L. Y. Chiu and B. M. Diong, "An improved small-signal model of the dynamic behavior of PEM fuel cells," *IEEE 38th IAS Ann. Meet.*, vol. 2, pp. 709–715, Oct. 2003.
[8] J. T. Pukrushpan, H. Peng, and A. G. Stefanopoulou, "Simulation and analysis of transient fuel cell system performance based on a dynamic reactant flow model," *Proc. of ASME IMECE'02*, 2002.
[9] S. Yerramalla, A. Davari, and A. Feliachi, "Dynamic modeling and analysis of polymer electrolyte fuel cell," *IEEE Power Eng. Soc. Summer Meet.*, vol. 1, pp. 82–86, Jul. 2002.
[10] J. T. Pukrushpan, A. G. Stefanopoulou, and H. Peng, "Modeling and control for PEM fuel cell stack system," *Am. Control Conf.*, vol. 4, pp. 3117–3122, May 2002.
[11] M. D. Lukas, K. Y. Lee, and H. Ghezel-Ayagh, "An explicit dynamic model for direct reforming carbonate fuel cell stack," *IEEE Trans. Energy Convers.*, vol. 16, pp. 289–295, Sep. 2001.
[12] D. J. Hall and R. G. Colclaser, "Transient modeling and simulation of a tubular solid oxide fuel cell," *IEEE Trans. Energy Convers.*, vol. 14, pp. 749–753, Sep. 1999.
[13] M. D. Lukas, K. Y. Lee, and H. Ghezel-Ayagh, "Development of a stack simulation model for control study on direct reforming molten carbonate fuel cell power plant," *IEEE Trans. Energy Convers.*, vol. 14, pp. 1651–1657, Dec. 1999.
[14] K. H. Hauer, "Dynamic interaction between the electric drive train and fuel cell system for the case of an indirect methanol fuel cell vehicle," *35th IECEC Meet.*, vol. 2, pp. 1317–1325, Jul. 2000.
[15] Y.-H. Kim and S.-S. Kim, "An electrical modeling and fuzzy logic control of a fuel cell generation system," *IEEE Trans. Energy Convers.*, vol. 14, no. 2, pp. 239–244, Jun. 1999.
[16] G. K. Andersen, C. Klumpner, S. B. Kjaer, and F. Blaabjerg, "A new green power inverter for fuel cells," *IEEE PESC'02*, vol. 2, pp. 727–733, Jun. 2002.
[17] R. Gopinath, S. Kim, J.-H. Hahn, M. Webster, J. Burghardt, S. Campbell, D. Becker, P. Enjeti, M. Yeary, and J. Howze, "Development of a low cost fuel cell inverter system with DSP control," *IEEE PESC'02*, vol. 1, pp. 309–314, Jun. 2002.
[18] A. M. Tuckey and J. N. Krase, "A low-cost inverter for domestic fuel cell applications," *IEEE PESC'02*, vol. 1, pp. 339–346, Jun. 2002.
[19] E. Santi, D. Franzoni, A. Monti, D. Patterson, F. Ponci, and N. Barry, "A fuel cell based domestic uninterruptible power supply," *IEEE APEC'02*, vol. 1, pp. 605–613, Mar. 2002.
[20] F. Z. Peng, "Z-source inverter," *IEEE Trans. Ind. Appl.*, vol. 39, no. 2, pp. 504–510, Mar.–Apr. 2003.
[21] J.-W. Jung and A. Keyhani, "Design of Z-source converter for fuel cells," *Electric Supply Industry in Transition, AIT Thailand*, 2004.
[22] P. Mattavelli, "A modified dead-beat control for UPS using disturbance observers," *IEEE PESC'02*, vol. 4, pp. 1618–1623, Jun. 2002.
[23] O. Kukrer, "Deadbeat control of a three-phase inverter with an output LC filter," *IEEE Trans. Power Electronics*, vol. 11, pp. 16–23, Jan. 1996.
[24] K. P. Gokhale, A. Kawamura, and R. G. Hoft, "Dead beat microprocessor control of PWM inverter for sinusoidal output waveform synthesis," *Conf. Record IEEE Power Elec. Spec. Conf.*, pp. 28–36, 1985.
[25] F. Botteron, H. Pinheiro, H. A. Grundling, J. R. Pinheiro, and H.L. Hey, "Digital voltage and current controllers for three-phase PWM inverter for UPS applications," *IEEE IAS'01*, vol. 4, pp. 2667–2674, 2001.
[26] E. J. Davison and B. Scherzinger, "Perfect control of the robust servomechanism problem," *IEEE Trans. Autom. Control*, vol. 32, no. 8, pp. 689–702, 1987.
[27] B. A. Francis and W. M. Wonham, "The internal model principle for linear multivariable regulators," *Appl. Math. Opt.*, vol. 2,, no. 2, pp. 170–194, 1975.
[28] V. Utkin, J. Guldner, and J. Shi, *Sliding Mode Control in Electromechanical Systems*. Philadelphia: Taylor & Franci, 1999.

Jin-Woo Jung (S'97–M'06) received the B.S. and M.S. degrees in electrical engineering from Hanyang University, Seoul, Korea in 1991 and 1997, respectively, and the Ph.D. degree in electrical and computer engineering from The Ohio State University, Columbus, OH, in 2005.

From 1997 to 2000, he was with Digital Appliance Research Laboratory, LG Electronics Company, Ltd., Seoul, Korea. Currently, He is with Corporate R&D Center, Samsung SDI Company, Ltd., Yongin, Gyeonggi-Do, Korea. His current research interests are in the area of distributed generation systems, driving circuits of ac plasma display panel (PDP), fuel cell systems, electric machines, ac motor drives, power converters, and control.

Ali Keyhani (S'69–M'72–S'72–M'76–SM'89–F'98) was with Hewlett-Packard Company and TRW Control from 1967 to 1972. Currently, he is a Professor of Electrical Engineering at the Ohio State University, Columbus, OH. He is the past Chairman of Electric Machinery Committee of IEEE Power Engineering Society and the past Editor of IEEE TRANSACTIONS ON ENERGY CONVERSION. He is the Director of Ohio State University Electromechanical and Mechatronic Systems Laboratory. His current research interests include the control of distributed energy systems, design and modeling of electric machine, control and design of power electronic systems, DSP-based virtual test bed for design, control of power systems, automotive systems, modeling, parameter estimation, and failure detection systems.

Dr. Keyhani is a recipient of the Ohio State University College of Engineering Research Award for 1989, 1999, and 2003